



ARTICLE

Advanced Poly(Lactic Acid)/Thermoplastic Polyurethane Blend-Based Nanocomposites with Carbon Nanotubes and Graphene Nanoplatelets for Shape Memory

Nayara Koba de Moura Morgado, Guilherme Ferreira de Melo Morgado, Erick Gabriel Ribeiro dos Anjos and Fabio Roberto Passador*

Department of Science and Technology, Polymer and Biopolymer Technology Laboratory (TecPBio), Federal University of São Paulo (UNIFESP), 330 Talim St, São José dos Campos, 12231-280, SP, Brazil

*Corresponding Author: Fabio Roberto Passador. Email: fabio.passador@unifesp.br

Received: 05 October 2024; Accepted: 17 January 2025; Published: 27 March 2025

ABSTRACT: The continuous improvement in patient care and recovery is driving the development of innovative materials for medical applications. Medical sutures, essential for securing implants and closing deep wounds, have evolved to incorporate smart materials capable of responding to various stimuli. This study explores the potential of thermoresponsive sutures, made from shape memory materials, that contract upon heating to bring loose stitches closer together, promoting optimal wound closure. We developed nanocomposites based on a blend of poly(lactic acid) (PLA) and thermoplastic polyurethane (TPU)—biopolymers that inherently exhibit shape memory—enhanced with carbon nanotubes (CNT) and graphene nanoplatelets (GN) to improve mechanical performance. PLA/TPU (50/50) nanocomposites were prepared with 1 and 2 wt% GN, as well as hybrid formulations combining 1 wt% CNT with 1 or 2 wt% GN, using a twin-screw extrusion process to form filaments. These filaments were characterized through differential scanning calorimetry (DSC), field emission gun scanning electron microscopy (FEG-SEM), tensile testing, and shape memory assessments. While the PLA/TPU blend is immiscible, TPU enhances the crystallinity (X_c) of the PLA phase, further increased by the addition of CNT and GN. FEG-SEM images indicate CNTs primarily in the PLA phase and GN in the TPU phase. PLA/TPU with 1 or 2 wt% GN showed the highest potential for suture applications, with a high elastic modulus (~1000 MPa), significant strain at break (~10%), and effective shape recovery (~20% at 55°C for 30 min). These findings suggest that these nanocomposites can enhance suture performance with controlled shape recovery that is suitable for medical use.

KEYWORDS: Shape memory polymers; poly(lactic acid) (PLA); thermoplastic polyurethane (TPU); carbon nanotubes (CNT); graphene nanoplatelets (GN)

1 Introduction

The constant progress in medicine and the development of materials for medical applications have led to safer and more effective surgical techniques. It is estimated that over 300 million major surgeries are performed worldwide annually, a number expected to increase with the growing global population [1]. With such a significant volume of surgeries, the demand for techniques and materials that promote better patient recovery becomes essential. Surgical procedures often require the use of medical sutures, which are critical for stabilizing implants and closing deep wounds to facilitate healing and prevent bleeding by compressing blood vessels [2,3].



Medical sutures have been used for approximately 3000 years BCE, employing materials such as animal tendons, guts, silk, and even cotton—all natural materials [4]. However, as material science advanced, particularly in the 20th century, natural materials were replaced by polymers like polypropylene (PP) and polyamide (Nylon[®]) [5]. This shift not only introduced new materials but also improved suture production techniques and surgical methods, leading to procedures that are less invasive, less painful, and associated with lower rates of inflammation and infection.

The selection of a suitable material for medical sutures is crucial, requiring biocompatibility to prevent inflammatory processes and avoid additional harm to wounds. For internal use, the material should also be biodegradable to eliminate the need for surgical removal and ensure non-toxic degradation within the body. As a result, the use of biopolymers, such as poly(lactic acid) (PLA), is highly recommended [6]. PLA stands out among biopolyesters due to its biocompatibility, biodegradability, ease of processing, high mechanical strength, and favorable degree of crystallinity [7,8]. However, being a rigid material, it may lack the flexibility needed for medical sutures applications.

An effective alternative to enhance the elasticity of PLA is the addition of a second phase through the development of polymer blends. The development of a polymer blend of PLA and thermoplastic polyurethane (TPU) addresses this concern, developing a material with improved flexibility, making it more suitable for medical sutures while retaining biocompatibility and mechanical strength [9]. The mechanical properties of TPU, which arise from its rigid and soft segments, provide excellent mechanical strength and elasticity, enabling it to be processed through thermoplastic techniques [10].

Another important property required for this application is shape memory, a response that allows the material to be programmed to recover its original state using external stimuli such as pH changes, electricity, light, or heat [11,12]. This thermoresponsive nature makes the PLA/TPU blend a smart material to aid in the healing process. When heated, the material contracts, potentially reducing the length of a medical suture and closing the wound [10]. This contraction is necessary during the healing process as it helps prevent the stitches from coming loose and keeps the wound closed [5,13–15].

Additionally, to leverage the innate shape memory response and avoid premature rupture, the mechanical properties of the PLA/TPU blend can be enhanced using nanofillers, such as carbon nanotubes (CNT) and graphene nanoplatelets (GN) [16–18]. Carbon nanofillers are highly recommended because they can produce nanocomposites with high specific mechanical strength when added in small quantities, typically below 5 wt% [19,20].

The combination of biopolymers such as PLA and TPU, along with the addition of carbon nanofillers like CNT and GN, results in a material with suitable mechanical strength, flexibility, and shape memory—properties that are advantageous for the development of advanced medical sutures.

In our previous work [21,22], we highlighted how the increasing demand for rapid patient recovery in surgical interventions has accelerated biomaterials research, leading to the development of shape memory polymers (SMP) like PLA/TPU blends with different blend ratios, which exhibit excellent shape memory properties, enhance wound healing, and demonstrate favorable mechanical characteristics for sutures; specifically, PLA/TPU (30/70) achieves an elongation at break of 80% and a shape recovery ratio of 40%. Additionally, our research on PLA/TPU (60/40) blends-based nanocomposites [21], enhanced with the addition of carbon nanomaterials, showed promising antimicrobial activity and an average shape recovery of approximately 6.5% in length, making these materials suitable for advanced antimicrobial sutures. The incorporation of carbon nanofillers can inhibit or manage the proliferation of pathogenic microorganisms and the onset of infectious processes in the suture area, while also enhancing the mechanical properties and shape memory effect of the suture thread [21].

In this work, a 50/50 PLA/TPU blend ratio was investigated, and the effects of adding carbon nanotubes (CNT) and graphene nanoplatelets (GN) on the thermal, mechanical, and shape memory properties were evaluated. The blend-based nanocomposites were prepared using an industrial-like, solvent-free method (extrusion), and the resulting filaments were characterized, demonstrating promising results for their application as medical sutures with good shape memory.

2 Methodology

2.1 Materials

PLA with specification PLI 005 (Nature Plast, Mondeville, France), MFI 25–35 g/10 min (190°C/2.16 kg), density of 1.25 g·cm⁻³, and Mw of 80,000 to 100,000 g·mol⁻¹.

TPU with specification Thermollan MXB 01 Natural from Eastman Scandiflex (São Paulo, Brazil) with a density of 1.21 g·cm⁻³, Shore A hardness of 80 ± 3, elongation at break ≈650%, and tear strength of 60 N·mm⁻¹.

Multiwalled carbon nanotubes (CNT) with specification NC7000 from Nanocyl SA (Sambreville, Belgium), produced through chemical catalytic vapor deposition (CCVD), with purity >90%, diameter of 9.5 nm, and length of 1.5 μm.

Graphene nanoplatelets (GN) from Cheaptube (Grafton, MA, USA) with purity >97%, average particle size >2 μm, and thickness between 8 and 15 nm.

2.2 Methods

2.2.1 Processing of PLA/TPU Blend-Based Nanocomposites

Filaments were produced using a twin-screw extruder AX Plásticos, model AX DR 16:40 (Diadema, São Paulo, Brazil) with a temperature profile of 170°C, 180°C, 185°C, 190°C, and 195°C (from the feeding zone to the matrix), along with a thread rotation speed of 80 rpm and feed speed of 25 rpm, using a double filament die. The polymers were dried for 24 h in an oven at 80°C before processing. The filaments were pulled at a constant speed to achieve a diameter of approximately 0.9 mm (commercial sutures have diameters ranging from 0.02 to 0.9 mm). The filament diameter was measured using a digital caliper at five different spots on each filament sample. The average diameter was found to be 0.9 mm, with a standard deviation (SD) of 0.1 mm.

Table 1 presents the compositions studied and the nomenclatures used in this work. These compositions were chosen for presenting good shape memory response and mechanical properties associated with the small content of the nanofillers according to results obtained by [11,21,22].

Table 1: Formulations of PLA/TPU blend-based nanocomposites with carbon nanotubes and graphene nanoplatelets

Samples	PLA (wt%)	TPU (wt%)	CNT (wt%)	GN (wt%)
PLA	100	0	0	0
50/50	50	50	0	0
50/50/CNT	50	50	1	0
50/50/GN1	50	50	0	1
50/50/GN2	50	50	0	2
50/50/CNT/GN1	50	50	1	1

(Continued)

Table 1 (continued)

Samples	PLA (wt%)	TPU (wt%)	CNT (wt%)	GN (wt%)
50/50/CNT/GN2	50	50	1	2
TPU	0	100	0	0

2.2.2 Thermal, Morphological, and Mechanical Tests

All characterizations were conducted directly on the prepared filaments.

Differential scanning calorimetry (DSC) was performed using Netzsch equipment, model 204 F1 Phoenix[®] (Berlin, Germany). The samples were subjected to one heating cycle from 25°C to 200°C (heating rate of 10°C·min⁻¹), an isotherm of 5 min, and cooled down to -80°C (cooling rate of 10°C·min⁻¹). The measurements were made using nitrogen as carrier gas with a continuous flow of 50 mL·min⁻¹. The degree of crystallinity (X_c) of PLA was obtained from the heating data by applying Eq. (1).

$$X_c = \frac{\Delta H_m - \Delta H_{cc}}{w_{PLA} \times \Delta H_m^0} \quad (1)$$

where ΔH_m is the fusion enthalpy of PLA, ΔH_{cc} is the cold crystallization enthalpy of PLA, ΔH_m^0 is the fusion enthalpy for 100% crystalline PLA (adopted as 93 J·g⁻¹ [23,24]) and w_{PLA} is the mass fraction of PLA.

The morphology of the samples was verified using the field emission gun scanning electron microscope (FEG-SEM). The filaments were cryofractured, placed in aluminum stubs, covered with a thin layer of gold, and observed using a Tescan microscope, model MIRA3 (Brno, Czech Republic), operating with 5 keV. The polymer blend-based compositions samples with TPU phase extraction were also evaluated by applying a methodology used by Jašo et al. [25], with the cryofracture surfaces immersed in dimethylformamide (DMF) for 5 min at room temperature.

The tensile tests were performed on filaments with 10 cm in length using a Universal Testing Machine MTS, model CRITERION 42 (Eden Prairie, MN, USA) with a load cell of 250 N and a speed rate of 50 mm·min⁻¹. Tensile tests were performed in a total of five replicates for each sample type.

2.2.3 Shape Memory Test

The shape memory effect was verified using a CORNING heating plate, model PC-420D (Corning Company, Corning, NY, USA) and a SOLAB stove, model SL-100/64 (SOLAB Científica, Piracicaba, São Paulo, Brazil). Fig. 1 illustrates the process of fixing and recovering the shape of the filaments. This procedure has been validated in previous works [20,21]. For each test configuration, five filaments samples were used.

For the shape memory assessment, filaments measuring 50 mm in length and 1 mm in diameter were heated to either 80°C or 100°C in a water bath containing distilled water. While submerged, the filaments were stretched to 100 mm using pliers at their tips. After being removed from the water bath, the filaments were held in the stretched position until they cooled to room temperature. The resulting elongation (ϵ_c) was then measured while the filaments remained under tension.

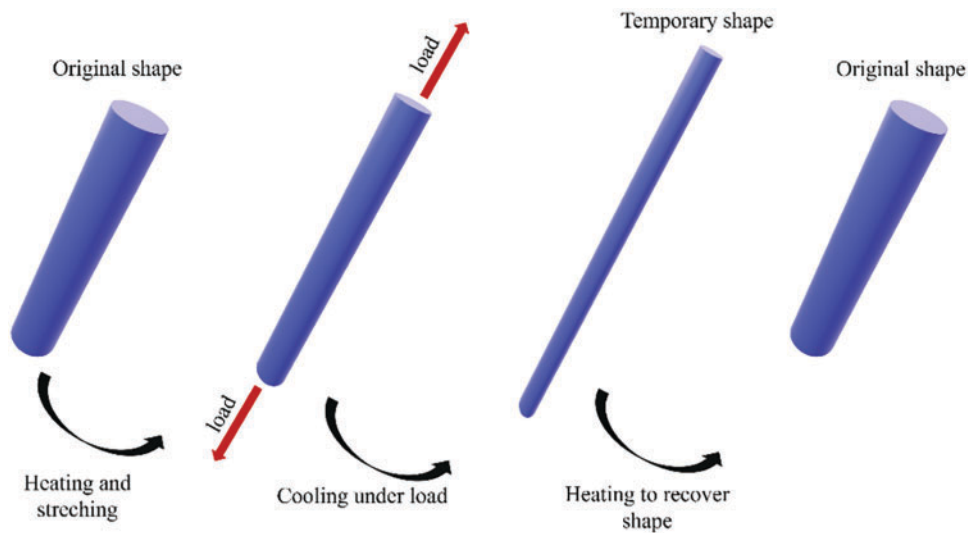


Figure 1: Schematic representation of shape memory mechanism in thermosensitive polymers. The polymer, in its original shape, that sample is heated and stretched to achieve the temporary shape, the sample is cooled down to fixate the temporary shape, and then the sample is heated again to recover the original shape

Subsequently, the pliers were removed, and the length of the filament was measured again to obtain the deformation after the fixing tension (ϵ), which was used to assess any shape recovery after the removal of strain. After cooling, the filaments maintained the stretched form without any significant recoil. The fixation rate (F_r) was calculated according to Eq. (2) to evaluate the capacity of the sample to retain deformation. To determine the recovery ratio at different temperatures, the filaments were heated in an oven for 30 min at different temperatures (37°C, 40°C, 55°C, and 70°C), and the final length of the filaments was measured, obtaining the deformation after recovery (ϵ_r). For each temperature, a recovery ratio (R_r) was calculated according to Eq. (3):

$$F_r = 100\% \times \frac{\epsilon}{\epsilon_c} \quad (2)$$

$$R_r = 100\% \times \frac{\epsilon_c - \epsilon_r}{\epsilon} \quad (3)$$

2.2.4 Statistical Analyzes

Statistical analyses were conducted on the obtained results to support this type of study. ANOVA (Analysis of Variance) was performed to determine the presence of significant differences between the results. Additionally, post-hoc Tukey's comparison test was applied to identify specific differences among the results. The significance level (α) used in these tests was 0.05.

3 Results and Discussion

3.1 Differential Exploratory Calorimetry

Fig. 2 presents the DSC curves, while Table 2 displays the transition temperature values obtained from the studied compositions.

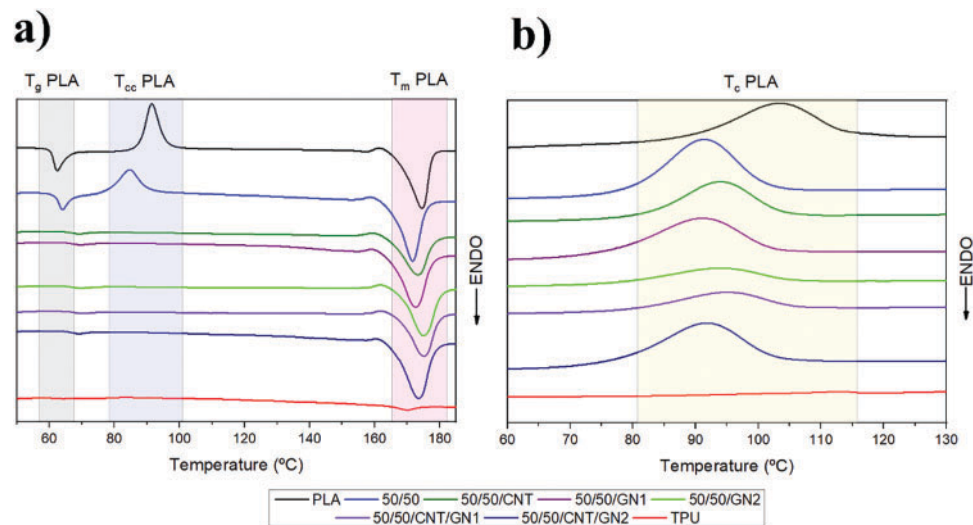


Figure 2: DSC curves for neat PLA, neat TPU, 50/50, and blend-based nanocomposites for (a) first heating and (b) cooling

Table 2: T_g , T_{CC} , T_m , and X_c obtained during first heating and T_c obtained during cooling of the PLA and PLA/TPU blend-based nanocomposites determined using DSC

Samples	T_g (°C) PLA	T_{cc} (°C) PLA	T_m (°C) PLA	X_c (%) PLA	T_c (°C) PLA
PLA	61	92	175	11	103
50/50	63	85	172	48	91
50/50/CNT	67	–	173	62	94
50/50/GN1	68	–	173	81	91
50/50/GN2	67	–	175	68	94
50/50/CNT/GN1	68	–	175	61	95
50/50/CNT/GN2	67	–	174	86	92
TPU	–	–	–	–	–

TPU is a polymer consisting of both soft and rigid segments. The TPU used in this study has a glass transition temperature (T_g) of -34°C for the soft segments, while PLA has a T_g of 61°C . The chosen temperature range was not aimed at TPU since PLA is the component responsible for the shape memory effect. Furthermore, we observed that the addition of nanofillers (CNT and GN) resulted in a slight increase in the T_g of PLA compared to the blends without nanofillers. This effect can be attributed to the improved interactions between the PLA phase and the nanofillers, which enhance the overall thermal properties of the material... Another observation is the increased degree of crystallinity (X_c) of the PLA phase with the incorporation of TPU and the nanofillers. Both the TPU phase and the nanofillers serve as heterogeneous crystallization sites for the PLA phase. As crystallinity increases, the available amorphous phase diminishes, which restricts the mobility of chain segments in this phase, requiring higher temperatures (and more energy) to mobilize the amorphous chains within the material [26].

The second thermal transition assessed was the cold crystallization temperature (T_{cc}) of PLA, which was noticeable only in neat PLA and PLA/TPU (50/50) samples. A possible hypothesis for the absence of T_{cc} could be the heterogeneous nucleation of the crystalline phase (lamellae), which promotes the formation

of a more crystalline phase and reduces the likelihood of cold crystallization during heating [27]. This is reflected in the substantial increase in the degree of crystallinity (X_c) observed in PLA/TPU blend and nanocomposites, where the presence of the TPU phase aids in heterogeneous nucleation, along with the nanofillers [28–30]. The highest values were found in compositions 50/50/GN1 (81%) and 50/50/CNT/GN2 (86%). Additional evidence supporting the heterogeneous nucleation hypothesis was observed in the crystallization temperature (T_c) of PLA, which decreased with the addition of TPU or nanofillers.

The TPU used is typically considered amorphous and does not show a significant endothermic peak transition. Additionally, the melting temperature (T_m) of PLA did not exhibit notable changes across the various compositions.

3.2 Morphological Characterization

Fig. 3a displays the surface of the cryofractured PLA filament, while Fig. 3b shows the surface of the cryofractured TPU filament. Since no additional material was incorporated into the precursor polymers, only one phase is observed in each case. Fig. 3c reveals the 50/50 blend, indicating a PLA matrix phase with a TPU dispersed phase in droplet form. This dispersion is homogeneous, exhibiting regular sizes and being well-distributed throughout the matrix. The lower viscosity of the PLA phase compared to that of the TPU phase favors the formation of a continuous phase. Based on these results, it can be affirmed that the PLA/TPU blend is an immiscible blend composed of two phases: the matrix phase is PLA, while the dispersed phase is TPU [31–33].

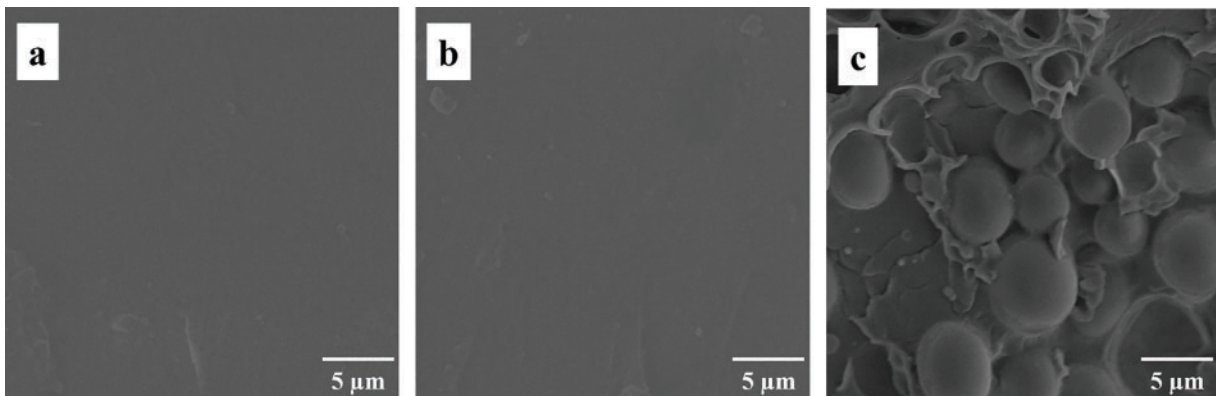


Figure 3: FEG-SEM images: (a) neat PLA, (b) neat TPU, (c) 50/50 blend, with a magnification of 10 kx

Fig. 4 shows the FEG-SEM images of the blend and nanocomposites. The morphology of the immiscible blend remains with the addition of nanofillers. Red arrows indicate some of the nanofillers present in the studied systems.

Previous studies report various preferences for the location of nanofillers in these systems; however, these preferences can vary depending on the type of CNT and GN, as well as the PLA and TPU phases involved. These factors contribute to the formation of unique systems, and while the literature can provide insights, it does not dictate these behaviors due to the numerous variables at play.

In Fig. 4a, a preferential location of dispersed CNTs in the PLA phase is observed, with no other dispersed filler observed in the evaluated region. For compositions 50/50/GN1 (Fig. 4b) and 50/50/GN2 (Fig. 4c), the selective location of GNs is observed primarily in the TPU phase, signed with red arrows and a red circle, which aligns with the predictions of the thermodynamic models, such as those proposed Wu's equation [34]. No dispersed nanofillers were observed in Fig. 4d,e which correspond to hybrid

nanocomposites in the evaluated region, possibly due to the encapsulation of nanofillers by the more elastomeric matrix. Ductile filament fracture is visible in Fig. 4d.

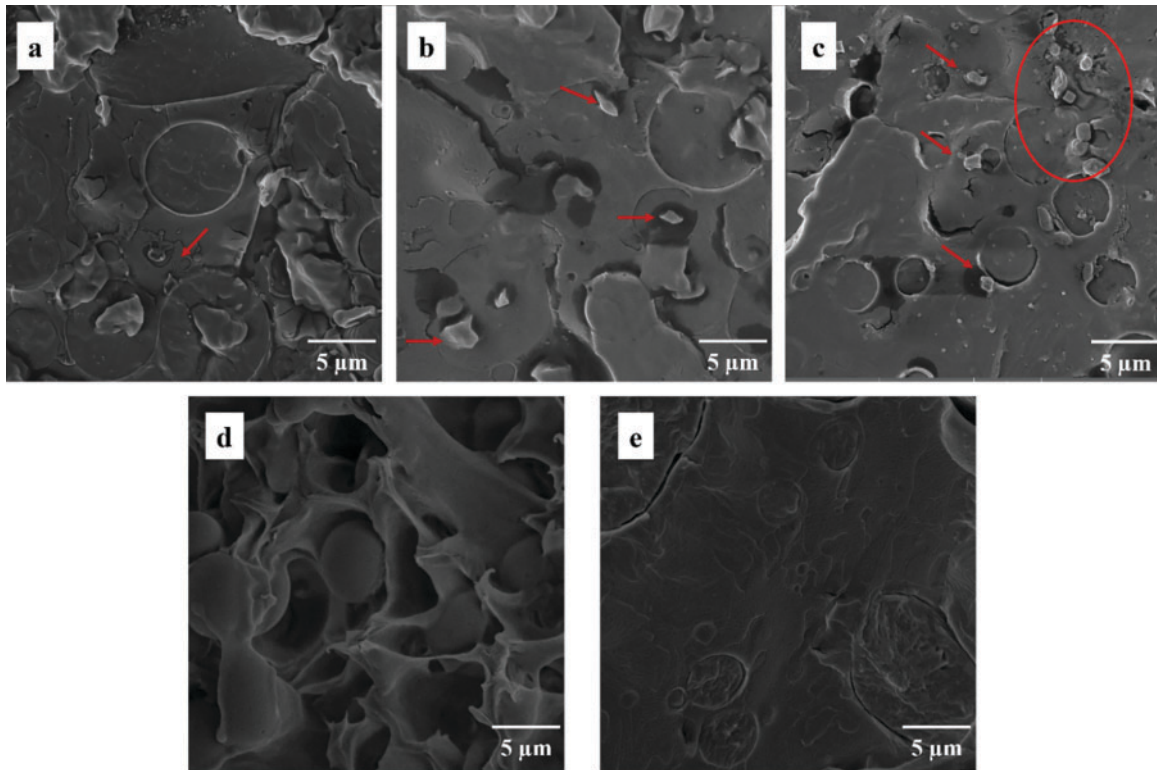


Figure 4: FEG-SEM images: (a) 50/50/CNT, (b) 50/50/GN1, (c) 50/50/GN2, (d) 50/50/CNT/GN1, and (e) 50/50/CNT/GN2, with a magnification of 10 kx

Fig. 5a shows an exposed CNT in the matrix, with an average diameter of approximately 50 nm. Fig. 5b presents GN with an average lateral size of 1.1 μm. Both fillers were measured using ImageJ software.

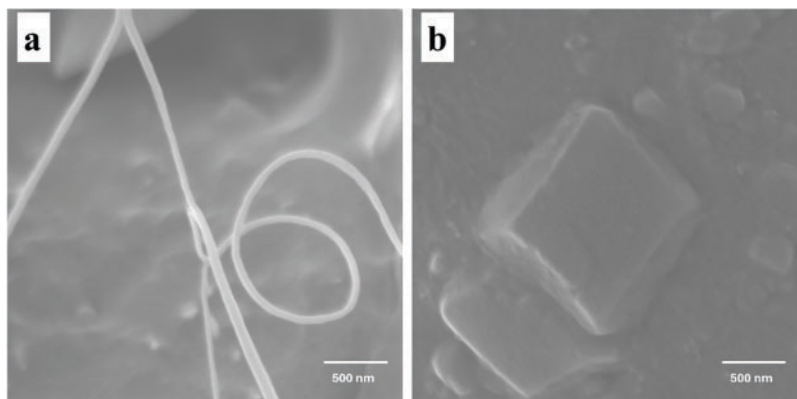


Figure 5: FEG-SEM images: (a) CNT and (b) GN in PLA/TPU matrix, with a magnification of 100 kx

Fig. 6 presents the FEG-SEM images of the blend and nanocomposites after the extraction of the TPU phase. The extraction aimed to identify the matrix and dispersed phases of the immiscible blend [25]. Initially, it was observed that the TPU phase, extracted using DMF, was indeed the dispersed phase, appearing as circular droplets, as shown in Figs. 3 and 4, for all studied compositions. As previously noted, an increase in TPU content in the blend composition resulted in larger dispersed droplets. Although the blend composition maintained equal mass quantities for PLA and TPU, only the presence of GN could be identified in Fig. 6, highlighted by the red circle. This observation suggests a possible preferential location of the nanofillers (CNT and GN) in the TPU phase, which was subsequently extracted.

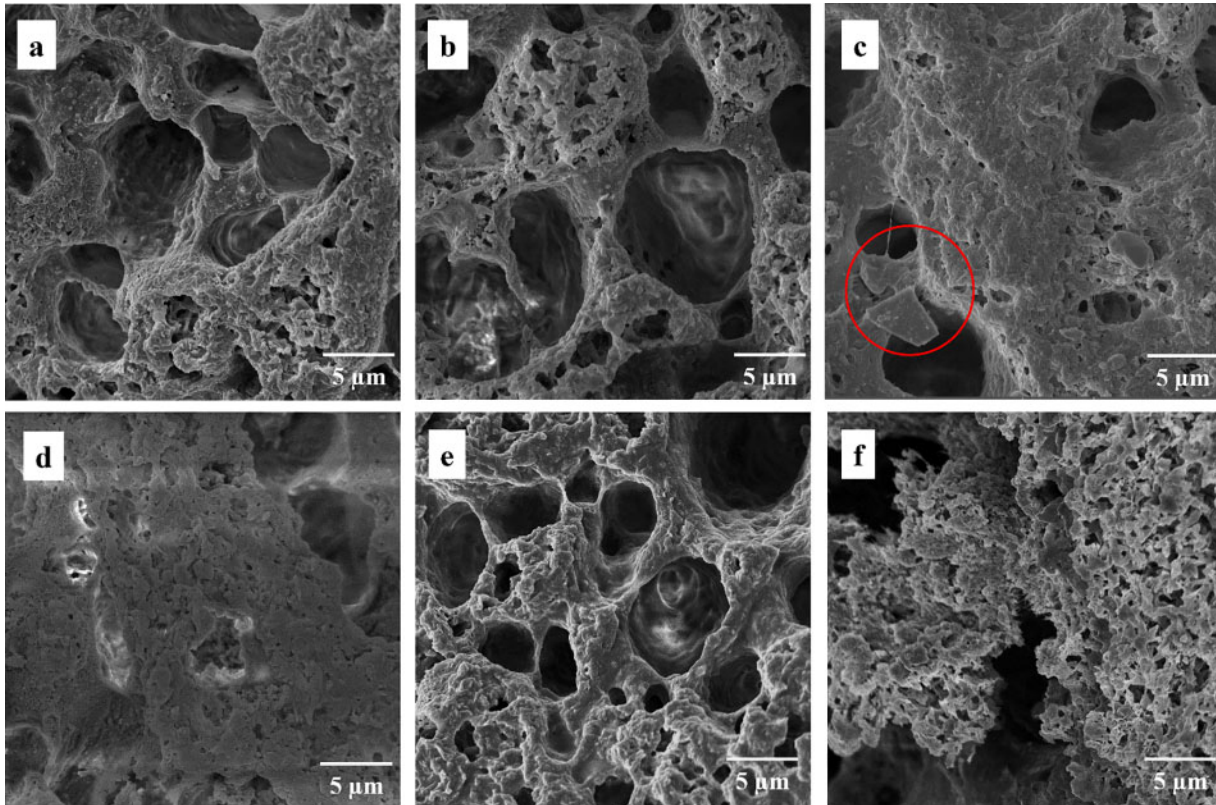


Figure 6: FEG-SEM images: (a) PLA/TPU blend (50/50), (b) 50/50/CNT, (c) 50/50/GN1, (d) 50/50/GN2, (e) 50/50/CNT/GN1, and (f) 50/50/CNT/GN2, after TPU phase extraction in DMF, with a magnification of 10 kx

3.3 Tensile Tests

According to the NBR 13904 and ISO 13485:2000 standards [35], which outline the requirements for non-absorbable surgical suture threads (Class I), it is recommended that these threads have a minimum tensile strength over a simple knot of approximately 88 N (39 MPa) for threads with a diameter of 0.9–0.999 mm, closely aligning with the obtained filaments diameter of 0.9 mm. Surgical suture threads typically exhibit high stretching capabilities, indicating enhanced mechanical properties. However, it is important to note that the stretching applied during in the conducted tests does not precisely replicate the actual stretching of suture threads in clinical settings. Therefore, these standards serve as a guide for evaluating the results.

Fig. 7 presents the stress-strain curves of the average behavior of the filaments. The values for ultimate tensile strength (UTS), deformation at break (ϵ_r), and elastic modulus (E) for the filaments are summarized in Table 3.

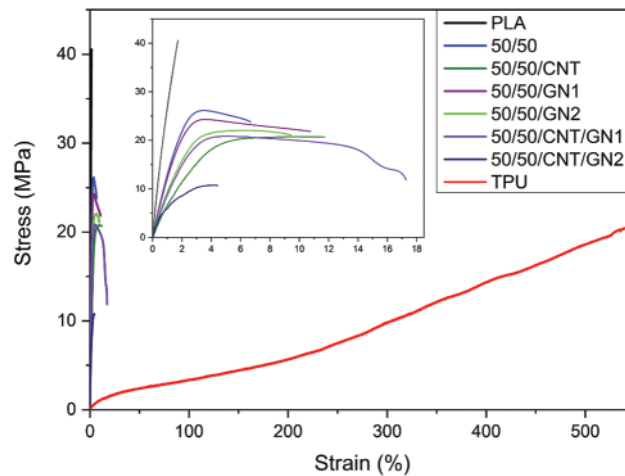


Figure 7: Stress x Strain curves of neat PLA, neat TPU, blend, and nanocomposites

Table 3: Ultimate tensile strength (UTS), deformation at the break, and elastic modulus obtained in the tensile test of the filaments of the studied compositions

Sample	UTS (MPa)	Deformation at break (%)	Elastic modulus (MPa)
PLA	40.5 ± 3.7 ^a	1.6 ± 0.5 ^d	2451.0 ± 234.9 ^a
50/50	25.6 ± 0.7 ^b	6.7 ± 0.7 ^c	1468.5 ± 90.0 ^a
50/50/CNT	21.1 ± 1.6 ^c	11.7 ± 1.8 ^b	946.3 ± 28.8 ^c
50/50/GN1	25.0 ± 0.6 ^b	10.8 ± 2.9 ^b	1256.1 ± 25.9 ^b
50/50/GN2	20.8 ± 1.6 ^c	9.4 ± 0.7 ^b	1114.6 ± 47.4 ^c
50/50/CNT/GN1	21.4 ± 0.4 ^c	17.6 ± 1.4 ^a	1070.6 ± 51.0 ^c
50/50/CNT/GN2	10.4 ± 0.5 ^e	4.1 ± 1.2 ^c	1022.1 ± 27.8 ^c
TPU	22.7 ± 1.5 ^c	>>650%*	6.8 ± 0.8 ^d

Note: Values followed by different letters indicate differences between 50/50 and their nanocomposites according to Tukey's test ($p < 0.05$). *Limit of the crosspiece of the equipment.

The addition of TPU in the composition resulted in the UTS values of the PLA/TPU blend (50/50) and its nanocomposites (average value of 22 MPa) approaching the value presented by neat TPU (23 MPa). The only exception was the composition 50/50/CNT/GN2, which exhibited a significantly lower value (10 MPa). This composition has the highest nanofiller content (3 wt%), where the nanofillers, especially GN, may begin to act as microcracks within the matrix phases [36], significantly reducing elongation.

All compositions containing TPU exhibited higher deformation at break than neat PLA, with the 50/50/CNT/GN1 composition being the most ductile (~18%), surpassing even neat TPU. The elastic modulus (E) of the PLA/TPU blend (50/50) (~1500 MPa) was higher than of the other nanocomposites (~1100 MPa), with the lowest E value observed in the 50/50/CNT composition (~950 MPa). These results align with literature findings, which suggest that the incorporation of TPU into PLA matrices enhances ductility while decreasing both the elastic modulus and UTS [37,38], highlighting the favorable performance of the PLA/TPU blend.

Furthermore, when comparing the deformation at break behavior of the PLA/TPU 50/50 blend with that of the nanocomposites containing 1 and 2 wt% of nanofillers, a notable increase in elongation from

6.7% to 9.4%–17.6% was observed. These improvements suggest that the addition of nanofillers is an effective strategy for enhancing the mechanical properties of the PLA/TPU blend. Similar effects have been previously reported, especially with the addition of GN in polymer blends [36]. This behavior may be attributed to the potential compatibilizing action of the nanofillers, which improves interactions between the PLA and TPU phases at low filler contents.

The hybrid composition containing 1 wt% of each nanofiller (CNT and GN) was particularly effective, likely due to the complementary shapes of the nanomaterials. Based on the results presented in Fig. 7 and Table 3, the 50/50/GN1 and 50/50/CNT/GN1 compositions exhibit excellent UTS and deformation at break values, suggesting their potential for shape memory applications.

3.4 Shape Memory

The recovery behavior of the compositions was evaluated at various recovery temperatures (37°C, 40°C, 55°C, and 70°C). Fig. 8 illustrates the recovery ratios as a function of recovery temperatures over 30 min. Notably, TPU exhibited the highest recovery among the evaluated compositions. A clear relationship can be established between the T_g of the materials and their shape recovery capacity, as observed through the Recovery Ratio (R_r).

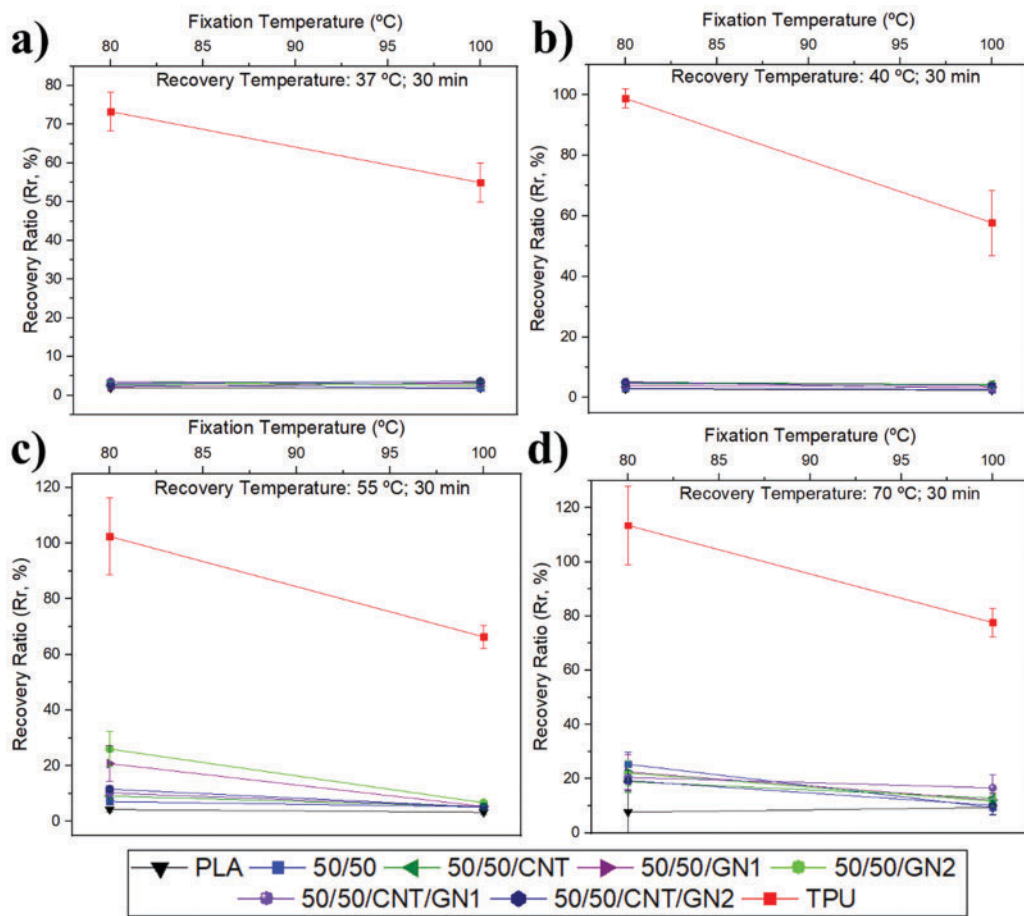


Figure 8: Recovery Ratio (R_r) in 30 min for shape fixation for all compositions, with recovery temperature at (a) 37°C, (b) 40°C, (c) 55°C, and (d) 70°C

At room temperature (25°C–27°C, with tests conducted in a controlled environment to minimize external influences), TPU is already above its T_g , allowing significant mobility of its polymer chains. This mobility suggests that TPU will exhibit good shape recovery when subjected to a temperature above room temperature, with the recovery ratio increasing as the recovery temperature rises [39–41].

Initially, for recoveries carried out at 37°C (simulating body temperature) and 40°C (chosen to simulate a feverish state), the recovery of compositions containing PLA was minimal (below 5%). This is directly related to the fact that these temperatures remain below the T_g of PLA. When the recovery temperature reached 55°C, an increase in recovery was observed for blends and nanocomposites (ranging between 5% and 10%), as this temperature is closer to the T_g of PLA. At 70°C (chosen to exceed the T_g of PLA), the recovery for PLA-based compositions ranged between 10% and 20%, which is a suitable values for the intended application since excessive recovery could risk rupturing the patient's skin.

The influence of material composition is also evident, with the 50/50/GN1 and 50/50/GN2 compositions containing GN (which act as lubricants) [19,20] showing higher recovery values (approximately 21.8%). These were followed by 50/50/CNT (17.6%) and 50/50 (16.8%), demonstrating that the addition of thermal conductive fillers positively impacts shape recovery [42,43].

Table 4 presents the R_r data for fixing temperature at 80°C, recovery temperatures at 37°C, 40°C, 50°C, and 70°C, and a recovery time of 30 min. It is important to note, as seen in Fig. 8, that all compositions showed a significant decrease in R_r when using a fixing temperature of 100°C; therefore, these data were not analyzed. Table 4 also presents de F_r (fixation rate), showing the capacity of the sample to retain the deformation.

Table 4: R_r in 30 min for shape fixation at 80°C, with recovery temperature at 37°C, 40°C, 55°C, and 70°C

Compositions	F_r (%)	R_r 37°C (%)	R_r 40°C (%)	R_r 55°C (%)	R_r 70°C (%)
PLA	99.6 ± 0.7 ^a	1.9 ± 0.1 ^b	2.9 ± 0.9 ^b	3.4 ± 1.9 ^d	29.6 ± 7.7 ^b
50/50	98.0 ± 0.9 ^a	2.6 ± 0.9 ^b	3.2 ± 0.7 ^b	7.2 ± 0.6 ^c	25.4 ± 4.4 ^b
50/50/CNT	98.4 ± 0.1 ^a	2.7 ± 0.8 ^b	5.1 ± 1.0 ^b	9.2 ± 2.7 ^c	19.0 ± 4.3 ^b
50/50/GN1	97.9 ± 0.6 ^a	2.1 ± 0.6 ^b	4.1 ± 0.8 ^b	20.8 ± 6.4 ^b	22.5 ± 6.4 ^b
50/50/GN2	98.3 ± 0.1 ^a	3.5 ± 0.2 ^b	4.8 ± 0.6 ^b	26.1 ± 6.2 ^b	22.1 ± 4.7 ^b
50/50/CNT/GN1	98.3 ± 0.1 ^a	3.6 ± 0.2 ^b	4.9 ± 0.8 ^b	10.3 ± 1.6 ^c	20.5 ± 2.5 ^b
50/50/CNT/GN2	98.3 ± 0.1 ^a	3.1 ± 0.6 ^b	4.9 ± 0.6 ^b	11.6 ± 1.3 ^c	19.3 ± 3.7 ^b
TPU	60.8 ± 1.9 ^b	73.3 ± 4.9 ^a	98.8 ± 3.1 ^a	102.5 ± 13.9 ^a	113.5 ± 14.4 ^a

Note: Values followed by different letters indicate differences among the studied compositions according to the Tukey test ($p < 0.05$).

According to Table 4, the R_r values for recovery at 37°C were statistically equal for all compositions, averaging 2.7%, except for TPU, which exhibited a substantially higher recovery (~70%). At 40°C, the compositions remained statistically similar, with an average R_r of around 4.1%, reflecting a slight increase in shape recovery capacity with the rise in temperature. TPU, however, showed a much higher recovery of 98.8%. The low shape recovery capacity observed in the compositions containing PLA is attributed to the T_g of PLA being above the recovery temperatures used.

For shape recovery at 55°C, the behavior shows noticeable changes. Neat PLA exhibits minimal recovery (3.4%), while neat TPU displays substantial recovery (102.5%). Notably, the 50/50/GN1 and 50/50/GN2 compositions demonstrate an average recovery of 23%, significantly higher than the other compositions,

which average around 8.6%. This enhanced recovery in the 50/50/GN1 and 50/50/GN2 compositions is linked to the lubricating effect of GN, which facilitates easier chain movement during recovery.

At 70°C, the recovery behavior shifts once more. Since this temperature exceeds the T_g of PLA, all compositions exhibit an increased recovery capacity, with R_r around 20%, showing no significant statistical difference among them, except for neat TPU, which presents a recovery of 113%. This high TPU recovery is likely due to the material's tendency to revert to its thermodynamically stable state. During filament processing, the orientation of TPU chains is influenced by shear rate, and at higher temperatures, the chain returns to its coiled configuration, resulting in greater length retraction [44].

The Fixation rate (F_f) is statistically equal for PLA, 50/50 polymer blend, and its nanocomposites, showing the influence of PLA in the shape memory effect. For TPU, the F_f is low, which is expected for materials that exhibit rubbery behavior.

4 Conclusion

The effects of adding CNT and GN on the thermal, mechanical, and shape memory properties of a 50/50 PLA/TPU matrix were successfully explored. The addition of these nanofillers enhanced the degree of crystallinity of the PLA phase and suppressed the cold crystallization phenomenon typically observed in PLA during heating. This was attributed to the heterogeneous nucleation effect of TPU and the nanomaterials, as evidenced by a reduction in the crystallization temperature of the nanocomposites. The morphology of the polymer blend confirmed the immiscibility of the PLA/TPU system, with strong indications of preferential location of GN in the TPU phase, further corroborated by TPU phase extraction analysis. From a mechanical perspective, the PLA/TPU 50/50 blend exhibited a remarkable balance of properties, exhibiting a high elastic modulus (~1500 MPa) compared to TPU, good deformation at break (6.7%) relative to PLA, and moderate tensile strength at low strain (~22 MPa). The addition of nanofillers enhanced phase interactions, resulting in a slight reduction in elastic modulus but significant increases in elongation, reaching 17.6% for the hybrid nanocomposites. Notably, GN exhibited a lubricating effect, contributing to a superior shape memory response, with an average recovery of 23% at 55°C, compared to the other nanocomposites and the polymer blend. These results provide practical insights into tuning the mechanical and shape memory properties of polymer blend-based materials for potential medical applications.

Acknowledgement: The authors would like to thank INPE (National Space Research Institute) for the FEG-SEM images.

Funding Statement: This study was financed in part by the Coordenação de Aperfeiçoamento de Pessoal de Nível Superior—Brasil (CAPES)—Finance Code 001.

Author Contributions: Study conception and design: Nayara Koba de Moura Morgado and Fabio Roberto Passador; Data collection: Nayara Koba de Moura Morgado and Guilherme Ferreira de Melo Morgado; Analysis and interpretation of results: Nayara Koba de Moura Morgado and Erick Gabriel Ribeiro dos Anjos; Draft manuscript preparation: Nayara Koba de Moura Morgado, Guilherme Ferreira de Melo Morgado and Erick Gabriel Ribeiro dos Anjos. All authors reviewed the results and approved the final version of the manuscript.

Availability of Data and Materials: The datasets generated and/or analyzed during the current study are available in the UNIFESP repository: <https://hdl.handle.net/11600/61101>, accessed on 10 January 2025.

Ethics Approval: Not applicable.

Conflicts of Interest: The authors declare no conflicts of interest to report regarding the present study.

References

1. Dobson GP. Trauma of major surgery: a global problem that is not going away. *Int J Surg*. 2020;81:47–54. doi:10.1016/j.ijssu.2020.07.017.
2. Pensalfini M, Meneghello S, Lintas V, Bircher K, Ehret AE, Mazza E. The suture retention test, revisited and revised. *J Mech Behav Biomed Mater*. 2018;77:711–7. doi:10.1016/j.jmbbm.2017.08.021.
3. Xu L, Liu Y, Zhou W, Yu D. Electrospun medical sutures for wound healing: a review. *Polymers*. 2022;14:1637. doi:10.3390/polym14091637.
4. Muffly TM, Tizzano AP, Walters MD. The history and evolution of sutures in pelvic surgery. *J R Soc Med*. 2011;104:107–12. doi:10.1258/jrsm.2010.100243.
5. Lekic N, Dodds SD. Suture materials, needles, and methods of skin closure: what every hand surgeon should know. *J Hand Surg Am*. 2022;47:160–71.e1. doi:10.1016/j.jhsa.2021.09.019.
6. Bibire T, Yilmaz O, Ghiciuc CM, Bibire N, Dănilă R. Biopolymers for surgical applications. *Coatings*. 2022;12:211. doi:10.3390/coatings12020211.
7. Kabir E, Kaur R, Lee J, Kim K-H, Kwon EE. Prospects of biopolymer technology as an alternative option for non-degradable plastics and sustainable management of plastic wastes. *J Clean Prod*. 2020;258:120536. doi:10.1016/j.jclepro.2020.120536.
8. Hamad K, Kaseem M, Yang HW, Deri F, Ko YG. Properties and medical applications of polylactic acid: a review. *Express Polym Lett*. 2015;9:435–55. doi:10.3144/expresspolymlett.2015.42.
9. Datta J, Kasprzyk P. Thermoplastic polyurethanes derived from petrochemical or renewable resources: a comprehensive review. *Polym Eng Sci*. 2018;58:E14–35. doi:10.1002/pen.24633.
10. Backes EH, Harb SV, Pinto LA, de Moura NK, de Melo Morgado GF, Marini J, et al. Thermoplastic polyurethanes: synthesis, fabrication techniques, blends, composites, and applications. *J Mater Sci*. 2024;59(4):1123–52. doi:10.1007/s10853-023-09077-z.
11. Lai SM, Lan YC. Shape memory properties of melt-blended polylactic acid (PLA)/thermoplastic polyurethane (TPU) bio-based blends. *J Polym Res*. 2013;20:2–9. doi:10.1007/s10965-013-0140-6.
12. Lendlein A. Shape-memory polymers. Berlin/Heidelberg, Germany: Springer; 2010. doi:10.1007/978-3-642-12359-7.
13. Mackenzie D. The history of sutures. *Med Hist*. 1973;17:158–68. doi:10.1017/S0025727300018469.
14. Kudur M, Pai S, Sripathi H, Prabhu S. Sutures and suturing techniques in skin closure. *Indian J Dermatol Venereol Leprol*. 2009;75:425. doi:10.4103/0378-6323.53155.
15. Vogels RRM, Lambert A, Schuster P, Jockenhoovel S, Bouvy ND, Disselhorst-Klug C, et al. Biocompatibility and biomechanical analysis of elastic TPU threads as new suture material. *J Biomed Mater Res B Appl Biomater*. 2017;105:99–106. doi:10.1002/jbm.b.33531.
16. Ivanov E, Kotsilkova R, Xia H, Chen Y, Donato RK, Donato K, et al. PLA/Graphene/MWCNT composites with improved electrical and thermal properties suitable for FDM 3D printing applications. *Appl Sci*. 2019;9(6):1209. doi:10.3390/app9061209.
17. Braga NF, dos Anjos EGR, de Moura NK, Silva TF, Passador FR. Polymer nanocomposites filled in carbon nanotubes: properties and applications. In: Myasoedova VV, Thomas S, Maria HJ, editors. *Chemical physics of polymer nanocomposites: processing, morphology, structure, thermodynamics, rheology*. 1st ed. Hoboken, NJ, USA: Wiley VCH; 2024. Vol. 1–3, p. 133–63.
18. Gao Y, Picot OT, Zhang H, Bilotti E, Peijs T. Synergistic effects of filler size on thermal annealing-induced percolation in polylactic acid (PLA)/graphite nanoplatelet (GNP) nanocomposites. *Nanocomposites*. 2017;3:67–75. doi:10.1080/20550324.2017.1333780.
19. Ferreira EHC, Andrade RJE, Fechine GJM. The superlubricity State of carbonaceous fillers on polyethylene-based composites in a molten State. *Macromolecules*. 2019;52:9620–31. doi:10.1021/acs.macromol.9b01746.
20. Garcia PS, de Oliveira YDC, Valim FCF, Kotsilkova R, Ivanov E, Donato RK, et al. Tailoring the graphene oxide chemical structure and morphology as a key to polypropylene nanocomposite performance. *Polym Compos*. 2021;42:6213–31. doi:10.1002/pc.26297.

21. de Morgado GFM, de Moura NK, Martins EF, Escanio CA, Backes EH, Marini J, et al. Effect of blend ratio on thermal, mechanical, and shape memory properties of poly(lactic acid)/thermoplastic polyurethane bio-blends. *J Polym Res.* 2022;29:533. doi:10.1007/s10965-022-03389-5.
22. de Moura NK, de Morgado GFM, Martins EF, Escanio CA, Esposito E, Marini J, et al. Evaluation of shape memory in Poly (lactic acid)/thermoplastic Polyurethane filaments with carbon nanotubes and graphene nanoplatelets. *Macromol Symp.* 2022;406:220020. doi:10.1002/masy.202200020.
23. Mo XZ, Wei FX, Tan DF, Pang JY, Lan CB. The compatibilization of PLA-g-TPU graft copolymer on polylactide/thermoplastic polyurethane blends. *J Polym Res.* 2020;27(2):33. doi:10.1007/s10965-019-1999-7.
24. Ribeiro Neto WA, Pereira IHL, Ayres E, de Paula ACC, Averous L, Góes AM, et al. Influence of the microstructure and mechanical strength of nanofibers of biodegradable polymers with hydroxyapatite in stem cells growth. Electrospinning, characterization and cell viability. *Polym Degrad Stab.* 2012;97:2037–51. doi:10.1016/j.polymdegradstab.2012.03.048.
25. Jašo V, Cvetinov M, Rakić SSS, Petrović ZS. Bio-plastics and elastomers from polylactic acid/thermoplastic polyurethane blends. *J Appl Polym Sci.* 2014;131(22):179. doi:10.1002/app.41104.
26. Makhlof ASH, Scharnweber D. Handbook of nanoceramic and nanocomposite coatings and materials. Oxford, UK: Butterworth-Heinemann; 2015.
27. Kahraman Y, Özdemir B, Kılıç V, Goksu YA, Nofar M. Super toughened and highly ductile PLA/TPU blend systems by *in situ* reactive interfacial compatibilization using multifunctional epoxy-based chain extender. *J Appl Polym Sci.* 2021;138(20):50457. doi:10.1002/app.50457.
28. Keramati M, Ghasemi I, Karrabi M, Azizi H, Sabzi M. Incorporation of surface modified graphene nanoplatelets for development of shape memory PLA nanocomposite. *Fibers Polym.* 2016;17:1062–8. doi:10.1007/s12221-016-6329-7.
29. Fernández MJ, Fernández MD. Effect of organic modifier and clay content on non-isothermal cold crystallization and melting behavior of polylactide/organovermiculite nanocomposites. *Polymers.* 2020;12(2):364. doi:10.3390/polym12020364.
30. Ceregatti T, Pecharki P, Pachekoski WM, Becker D, Dalmolin C. Electrical and thermal properties of PLA/CNT composite films. *Rev Mater.* 2017;22(3):e11863. doi:10.1590/S1517-707620170003.0197.
31. Jing X, Mi HY, Peng XF, Turng LS. The morphology, properties, and shape memory behavior of Poly(lactic acid)/Thermoplastic Polyurethane blends. *Polym Eng Sci.* 2015;55:70–80. doi:10.1002/pen.23873.
32. Lin W, Qu JP. Enhancing impact toughness of renewable poly(lactic acid)/Thermoplastic polyurethane blends via constructing cocontinuous-like phase morphology assisted by Ethylene-Methyl Acrylate-Glycidyl Methacrylate Copolymer. *Ind Eng Chem Res.* 2019;58:10894–907. doi:10.1021/acs.iecr.9b01644.
33. Wang J, Zhang Y, Sun W, Chu S, Chen T, Sun A, et al. Morphology evolutions and mechanical properties of *In Situ* Fibrillar Poly(lactic acid)/Thermoplastic polyurethane blends fabricated by fused deposition modeling. *Macromol Mater Eng.* 2019;304(7):1900107. doi:10.1002/mame.201900107.
34. Ray SS, Salehiyan R. Effects associated with constituents. Nanostructured immiscible polymer blends. Centro Rio de Janeiro, Brazil: Elsevier; 2020. p. 143–59. doi:10.1016/b978-0-12-816707-6.00008-0.
35. Associação Brasileira de Normas Técnicas. ABNT Standard NBR13904, 2003. In: Fios para sutura cirúrgica. Salvador, Brazil: ABNT; 2003.
36. Pour RH, Hassan A, Soheilmoghaddam M, Bidsorkhi HC. Mechanical, thermal, and morphological properties of graphene reinforced polycarbonate/acrylonitrile butadiene styrene nanocomposites. *Polym Compos.* 2016;37:1633–40. doi:10.1002/pc.23335.
37. Sun H, Hu J, Bai X, Zheng Z, Feng Z, Ning N, et al. Largely improved toughness of poly(lactic acid) by unique electrospun fiber network structure of thermoplastic polyurethane. *Polym Test.* 2017;64:250–3. doi:10.1016/j.polymertesting.2017.10.012.
38. Varsavas SD, Kaynak C. Effects of glass fiber reinforcement and thermoplastic elastomer blending on the mechanical performance of polylactide. *Compos Commun.* 2018;8:24–30. doi:10.1016/j.coco.2018.03.003.
39. Boyacioglu S, Kodal M, Ozkoc G. A comprehensive study on shape memory behavior of PEG plasticized PLA/TPU bio-blends. *Eur Polym J.* 2020;122:109372. doi:10.1016/j.eurpolymj.2019.109372.

40. Lai SM, Wu WL, Wang YJ. Annealing effect on the shape memory properties of polylactic acid (PLA)/thermoplastic polyurethane (TPU) bio-based blends. *J Polym Res.* 2016;23:1–13. doi:10.1007/s10965-016-0993-6.
41. Dogan SK, Boyacioglu S, Kodal M, Gokce O, Ozkoc G. Thermally induced shape memory behavior, enzymatic degradation and biocompatibility of PLA/TPU blends: effects of compatibilization. *J Mech Behav Biomed Mater.* 2017;71:349–61. doi:10.1016/j.jmbbm.2017.04.001.
42. Meng Q, Hu J. A review of shape memory polymer composites and blends. *Compos Part A Appl Sci Manuf.* 2009;40:1661–72. doi:10.1016/j.compositesa.2009.08.011.
43. Liu T, Huang R, Qi X, Dong P, Fu Q. Facile preparation of rapidly electro-active shape memory thermoplastic polyurethane/poly lactide blends via phase morphology control and incorporation of conductive fillers. *Polymer.* 2017;114:28–35. doi:10.1016/j.polymer.2017.02.077.
44. Lan B, Li P, Luo X, Luo H, Yang Q, Gong P. Hydrogen bonding and topological network effects on optimizing thermoplastic polyurethane/organic montmorillonite nanocomposite foam. *Polymer.* 2021;212:123159. doi:10.1016/j.polymer.2020.123159.